Advances in Science and Technology Research Journal

Advances in Science and Technology Research Journal 2024, 18(1), 61–75
https://doi.org/10.12913/22998624/175930
ISSN 2299-8624, License CC-BY 4.0

Received: 2023.11.21
Accepted: 2024.01.05
Published: 2024.01.19

Computational Methods of the Identification of Chaboche Isotropic-Kinematic Hardening Model Parameters Derived from the Cyclic Loading Tests

Marta Wójcik[1*], Andrzej Gontarz[2], Andrzej Skrzat[1], Grzegorz Winiarski[2]

[1] Department of Materials Forming and Processing, Faculty of Mechanical Engineering and Aeronautics, Rzeszow University of Technology, Al. Powstańców Warszawy 8, 35-959 Rzeszów, Poland

[2] Department of Metal Forming, Faculty of Mechanical Engineering, Lublin University of Technology, Nadbystrzycka 36, 20-618 Lublin, Poland

* Corresponding author's e-mail: m.wojcik@prz.edu.pl

ABSTRACT

The Chaboche-Lemaitre combined isotropic-kinematic hardening model (CKIH) gives an overall information about the material behaviour under cyclic loading. The identification of hardening parameters is a difficult and time-consuming problem. The procedure of the parameters identification using the experimental hysteresis curve obtained in a cyclic loading test under strain control is presented in details here for a S235JR construction steel. The last stabilized cycle extracted from the hysteresis curve is required for the identification of hardening parameters. The model with three backstresses is tested here. The optimization algorithm is also used for the improvement of the agreement between experimental and numerical data. In order to include some uncertainty of experiment and the identification procedure, the authorial algorithm written on the basis of the fuzzy logic soft-computing method is applied here. The results obtained show that the identification procedure presented in this paper ensures the good agreement between the experimental tests and numerical calculations. The correct selection of parameters associated with the hardening is essential for the right description of material behaviour subject to loading in different engineering problems, including in metal forming processes.

Keywords: Chaboche isotropic-kinematic hardening model, kinematic hardening, isotropic hardening, cyclic loading, construction steel.

INTRODUCTION

Cyclic loading is a type of loading that often results in the propagation of cracks in structures caused by the repeated loads. Many buildings are classified to a high or super high cycle loading fatigue classes in which fatigue causes structural damages [1]. It influences on their performance and the lifespan of buildings, as well as, their safety of the use. Therefore, the previous numerical simulations in order to predict the elastic-plastic material response under cyclic loading beyond the plastic limit is essential to design structures and their usage. Cyclic loading should be also taken into consideration not only in the construction sector but also in metal forming processes. For example, severe plastic deformations (SPD) are characterized by the large plastic deformation and the omission of the cyclic loading during their analysis can lead to the wrong results.

However, the numerical simulations of cyclic loading tests require the proper selection of material model which gives a multipurpose description of the material response. Over years, different models have been used in order to predict the cyclic response of materials, for example: bilinear [2], multilinear [3], Frederick-Armstrong (F-A) [4], Chaboche [5], Ohno-Wang [6], Abdel-Karim Ohno [7], Norton-Bailey [8] and Prager [9] models. The Chaboche model is often

used in order to model the plasticity of different materials. It was firstly proposed by Chaboche as the development of the Frederick-Armstrong model by the addition of the superposition of some backstresses with different properties. The Chaboche kinematic hardening model is sometimes modified by the addition of the component associated with the isotropic hardening (Chaboche combined isotropic-kinematic hardening model – CIKH). Due to the superposition of some backstresses, the Chaboche model is also applied for considering the cyclic loading phenomena, e.g. ratcheting, stress relaxation or elastic and plastic shakedown [10-12]. The examples of the application of the Chaboche and CIKH models are contained in [13-16].

The use of both original and modified Chaboche models for modelling the behaviour of the material under cyclic loading has many advantages. For example, the CIKH model including both isotropic and kinematic hardening requires only four (for two backstresses) or six (for three backstresses) parameters associated with the kinematic hardening, two isotropic and some elastic parameters for most engineering applications. Additionally, the hardening parameters might be determined in uniaxial cyclic tension/compression tests. Therefore, the number of experimental research might be reduced to the minimum.

Although the number of parameters is relatively small in the Chaboche model and its modifications, the identification of backstresses is a difficult challenge which often requires solving the optimization problem in order to fit experimental and numerical hysteresis curves. Another limitation is that backstress components – and are not directly related to the physical quantifies, thus their identification is performed for specific purposes. The correct set of hardening parameters should predict the material behaviour under cyclic loadings in the best way. The CIKH model does not also include the non-proportional hardening and the strain memory [17].

Recently, the proper determination of a set of parameters for the Chaboche model or one of its modified ones has been taken under consideration. Different approaches dedicated to identification of hardening parameters are available in the literature. Liu at al. [18] used strain-controlled cycling loading tests at different strain amplitudes and ratcheting ones in order to verify the set of hardening parameters for Chaboche model. In [19], the strain-controlled tests are applied to determine kinematic and hardening parameters. In the previous works of authors [20, 21], the strain-controlled % cyclic loading tests were made in order to identity hardening parameters for the F-A and Chaboche-Lemaitre model for an aluminum alloy. The uniaxial and biaxial ratcheting tests are used for the verification of Chaboche hardening parameters in [22-26].

It is worth highlighting that hardening parameters might be determined only with a certain precision associated with both error in the prediction of experiment, as well as, errors in the identification process. In order to minimize the differences between experimental and numerical results, as well as, to improve the results of the identification process, the optimization problem is considered. The different optimization procedures in the identification of the Chaboche hardening parameters are presented in [27-35]. The hardening parameters procedures using advanced approaches based on genetic algorithms are also tested [36-38]. In the previous works, the authorial identification procedure using the fuzzy logic theory is described [39]. The approach includes the scattering of the input and output data, as well as, the influence of elastic-plastic differential equations, which are the mapping model, on the identification procedure. In contrast, it is not included in the classical optimization method.

The aim of this research is the identification of the set of hardening parameters using the Chaboche-Lemaitre isotropic-kinematic hardening model (CIKH) for the S235JR construction and machine steel, which is commonly applied in many engineering applications, also in a construction sector. Such identification is very important for the right prediction of the material behaviour in different, even catastrophic situations caused by the cyclic loading. Different identification procedures of hardening parameters (the last stabilized cycle method, the procedure proposed by Santus et al. [40]) based on the experimental strain-controlled cyclic loading tests are tested here. The procedures are focused on the stabilized cycles of hysteresis loops. The optimization procedure using both least-square method and the authorial fuzzy logic approach are then applied for the improvement of the agreement between the numerical and experimental data. The achievement of a good convergence between numerical and experimental results confirms the correctness of the selection of the hardening parameters.

CONSTITUTIVE EQUATIONS OF THE CIKH MODEL

The main constitutive equations associated with the classical plasticity and the Chaboche-Lemaitre isotropic-kinematic hardening model (CIKH) for a three dimensional (3-D) problem is described below.

– The strain tensor consists of the elastic and plastic components (Eq. 1):

$$\varepsilon = \varepsilon^e + \varepsilon^p \tag{1}$$

where: ε^e, ε^p and ε mean elastic, plastic and overall strain, respectively.

– In the incremental form used in calculations in order to identity the hardening parameters, the Eq. 1 might be rewritten (Eq. 2):

$$d\varepsilon = d\varepsilon^e + d\varepsilon^p \tag{2}$$

where: $d\varepsilon$, $d\varepsilon^e$ and $d\varepsilon^p$ describe the increment of overall, elastic and plastic strain, accordingly.

– The incremental Hook's law is written as follows (Eq. 3):

$$d\sigma = Cd\varepsilon^e \tag{3}$$

where: $d\sigma$ is the stress increment, C is the elastic, constitutive stiffness matrix.

– The evolution of the yield surface using the von Mises yield criterion assuming isotropic and kinematic hardening is described in line with Eq. 4:

$$f(\sigma,\chi,p) = \sqrt{\frac{3}{2}(\sigma_D - \chi)\cdot(\sigma_D - \chi)} - \sigma_y - r(p) \tag{4}$$

where: σ_D is the deviatoric part of the stress tensor, χ is a backstress tensor associated with the translation of the center of the yield surface, $r(p)$ is the isotropic hardening function related to the increase of the yield surface, σ_y is the yield stress and dp is the effective plastic strain.

For the plastic flow, the value of the $f(\sigma,\chi,p)$ formula is above or equals zero.

– The effective plastic strain dp, which is related to the isotropic hardening for a 3-D case is as follows (Eq. 5):

$$dp = \sqrt{\frac{2}{3}d\varepsilon^p \cdot d\varepsilon^p} \tag{5}$$

– In line with the normality condition, the plastic strain increment might be written as follows (Eq. 6):

$$d\varepsilon^p = d\lambda\frac{df}{d\sigma} \tag{6}$$

where: $d\lambda$ is the plastic multiplier and $\frac{df}{d\sigma}$ defines the normal to the yield surface (n). The formula above might be rewritten, therefore (Eq. 7).

$$d\varepsilon^p = d\lambda n \tag{7}$$

– The consistency condition might be written as follows (Eq. 8):

$$df(\sigma,x,p) = \frac{\partial f}{\partial\sigma}\cdot d\sigma + \frac{\partial f}{\partial\chi}\cdot d\chi + \frac{\partial f}{\partial p}dp = 0 \tag{8}$$

Eq. 8 assumes both isotropic and kinematic hardening of a material.

– According to the Chaboche model, the backstress is a sum of i additive partial backstress components (Eq. 9) and the evolution of each of them might be written according to the equation based on the F-A hardening rule (Eq. 10) [41]:

$$\chi = \sum_{i=1}^{n}\chi_i \tag{9}$$

$$d\chi_i = \frac{2}{3}C_i d\varepsilon^p \pm \gamma_i\chi_i|d\varepsilon^p| \tag{10}$$

where: C_i and γ_i are linear and rate coefficients which have a positive value. Depending on the sign of $d\varepsilon^p$ (increasing or decreasing load), Eq. 10 can be divided into two first-order linear, differential forms (Eq. 11-12) [40]:

$$\frac{d\chi_i}{d\varepsilon^p} = \frac{2}{3}C_i - \gamma_i\chi_i \text{ for } d\varepsilon^p > 0 \tag{11}$$

$$\frac{d\chi_i}{d\varepsilon^p} = \frac{2}{3}C_i + \gamma_i\chi_i \text{ for } d\varepsilon^p < 0 \tag{12}$$

Equations 10-11 can be solved as a Cauchy initial value problem. The evolution of χ_i is simulated with respect to ε^p, using its known initial value. The behaviour of χ_i is determined using Eq. 10 or 11, depending on the sign of $d\varepsilon^p$. During the cyclic loading tests, the hysteresis loops are generated and the material indicates the hardening effect and then the stabilization. It is noted that χ_i backstress components are contained between two asymptotes which describe the equilibrium points χ_i^{min} and χ_i^{max} (Eq. 13-14) [40-42], depending on that the material is loaded or unloaded. The equilibrium points are never reached (Fig. 1).

$$\lim_{\varepsilon^p\to\infty}\chi_i = \chi_i^{max} = \frac{C_i}{\gamma_i} \text{ if } \varepsilon^p >> \varepsilon_0^p \tag{13}$$

$$\lim_{\varepsilon^p\to\infty}\chi_i = \chi_i^{min} = -\frac{C_i}{\gamma_i} \text{ if } \varepsilon^p << \varepsilon_0^p \tag{14}$$

where: ε_0^p is initial value of plastic strain.

The size of a yield surface depends on the isotropic hardening. If the isotropic hardening is not

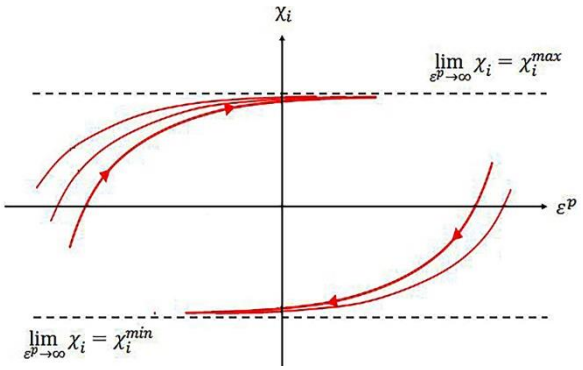

Figure 1. Asymptotes defining the equilibrium points for the backstress

observed, the yield stress is constant [41]. Otherwise, the yield surface expands uniformly. In this paper this assumed that it evolves in line with the Voce exponential formula (Eq. 15):

$$\sigma_y = \sigma_{y,0} + Q(1 - e^{-bp}) \tag{15}$$

where: $\sigma_{y,0}$ is the initial yield stress, Q is a multiplicative Voce's equation parameter, b is an exponential Voce's equation one, Q – parameter determines the saturation of the isotropic hardening and its variation might be positive for cyclic hardening or negative for cyclic softening [43], b – parameter describes the saturation rate [44].
It is assumed that (Eq. 16-17):

$$\sigma_y = \sigma_{y,0} + Q \text{ if } p \to \infty \tag{16}$$

$$\sigma_{y,0} - \sigma_y(p \to \infty) = -Qe^{-bp} \tag{17}$$

When the load is monotonic, isotropic and kinematic hardening behaves similarly. Under the cyclic loading, isotropic hardening cannot simulate the Bauschinger effect associated with the translation of a yield surface [45]. When the material is expected to be under cyclic loading, then kinematic hardening should be also used in numerical simulations. Using the equations presented above, the Chaboche-Lemaitre isotropic-kinematic hardening (CIKH) model can be used both to solved direct or inverse problems. The material and experimental parameters are input data and the stress-strain history is an output in solving of a direct problem. In the inverse problem, the experimental data is an input and hardening parameters are used as an output.

Procedure for identification of hardening parameters

The CIKH parameters are determined for the right prediction of the material behaviour in different engineering problems, with respect to the experimental results. The identification procedure used in this paper is considered as the inverse problem and is described in this section.

Before the determination of hardening parameters for the CIKH model, the maximum number of "*i*" backstresses should be selected. There are some tips how the best number of backstresses is chosen. It is assumed that the number of χ_i backstresses in the model should be the minimum but it should be sufficient to map the experiment as accurately as possible. In [46], three backstress components should be used for right modelling of cyclic loading tests (Fig. 2). The first χ_1 component should be highly nonlinear and it starts hardening with a large modulus indicating the quick stabilization. The second backstress χ_2 should model the transient non-linear part of a stable hysteresis loop. It should be also non-linear. The third χ_3 backstress component might be linear ($\gamma_3 = 0$) or almost linear ($\gamma_3 \to 0$). It describes the linear part of a hysteresis curve at high strains. Generally, it is assumed that $\gamma_1 > \gamma_2 > \gamma_3$. The selection of number linear and non-linear backstress components is arbitrary. Chaboche in [47] recommended the application of two non-linear and one linear components in order to control the tangent modulus at high strains. In [48], the small nonlinearity of the third backstress ($0 < \gamma_3 < 9$) is recommended to model the tangent modulus. It is also shown that the number of backstresses above three is not necessary and the application of their higher number does not improve the fitting of experimental and numerical results [49-51].

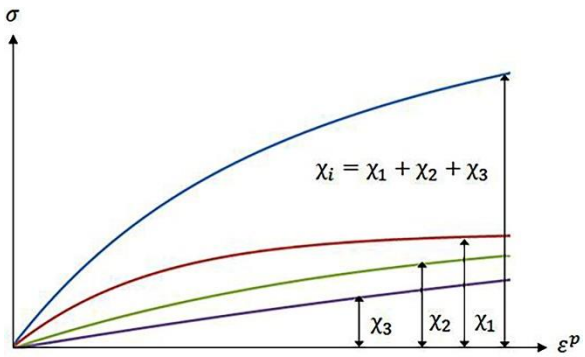

Figure 2. Interpretation of three backstresses components

The CIKH model with three backstress components and isotropic hardening described by the exponential Voce formula is applied in this paper. The set of eight parameters – two associated with the isotropic hardening (Q and b) and six related to the kinematic one ($C_1, C_2, C_3, \gamma_1, \gamma_2, \gamma_3$); are

identified to simulate the material behaviour under cyclic loading.

Firstly, kinematic hardening parameters for the CIKH model were selected. The stabilized hysteresis loop stress-strain data was applied here. It is a procedure using the data for the last stabilized cycle of the hysteresis curve in which the saturation of the isotropic hardening is observed. The method is applied mainly for long-term cycle analyses with several hysteresis loops. The steps for this procedure are as follows:

1) The last stabilized loop is extracted from the stress-strain hysteresis curve obtained in cyclic loading tests under strain-controlled conditions.
2) The data pair $(\sigma_i, \varepsilon_i^{pl})$ for the loop are determined with the strain axis shifted to ε_0^{pl} (Eq. 18) (Fig. 3):

$$\varepsilon^p{}_i = \varepsilon_i - \frac{\sigma_i}{E} - \varepsilon^p{}_0 \tag{18}$$

where: $\varepsilon^p{}_0$ means the transfer of the yield surface. For the first point of the loop, $\varepsilon^p{}_1 = 0$, therefore.

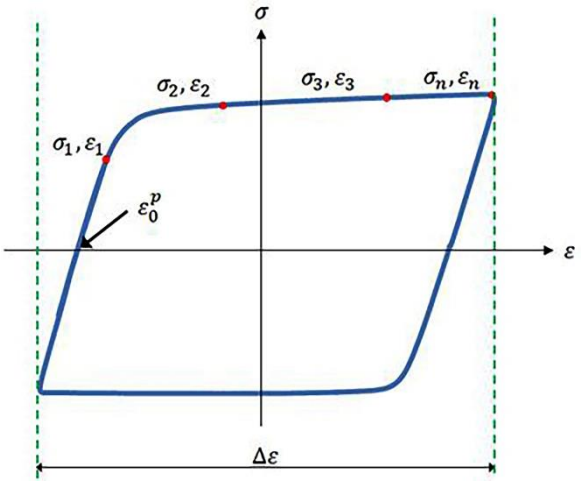

Figure 3. The exemplary last stabilized cycle used in a procedure for parameter identification

3) For each data pair $(\sigma_i, \varepsilon_i^{pl})$, the values of χ_i are determined using the experimental data (Eq. 19):

$$\chi_i = \sigma_i - \sigma^s \tag{19}$$

where: σ^s determines the size of the yield surface after the stabilization (Eq. 20):

$$\sigma^s = \frac{\sigma_1 + \sigma_n}{2} \tag{20}$$

4) Based on the backstress evolution law in the integrated form and assuming that $\varepsilon^p{}_1 = 0$ for the first data pair, it can be written that (Eq. 21):

$$\chi_i = \frac{C_i}{\gamma_i}\left(1 - e^{-\gamma_i \varepsilon^p}\right) \tag{21}$$

The equation above is then used for the determination of C_i and γ_i parameters for the CIKH model. The isotropic hardening parameters were then identified on the basis of the first and the last stabilized hysteresis loops extracted from the experimental stress-strain curve. The Q isotropic parameter is determined as follows (Eq. 22):

$$Q = \sigma_{y\,(p\to\infty)} - \sigma_0 \tag{22}$$

The second isotropic parameter b describing the rate of the yield stress increasing, is calculated as follows (Eq. 23):

$$b = -\frac{ln\frac{\sigma_{y\,(p\to\infty)} - \sigma_0}{Q}}{p} \tag{23}$$

It is assumed that the value of b parameter depends on the material saturation rate. The high values of b parameter are obtained for the fast stabilization of the material [52]. On the basis of the steps presented above, the algorithm is written in a commercial program and is used here.

The second approach for the identification of kinematic hardening parameters is the procedure proposed by Santus et al. [40]. The stabilized cycles of two cyclic stress-strain curves obtained in symmetrical and non-symmetrical cyclic loading tests are used here – for $\varepsilon = -0.5 \div 1\%$ and $\varepsilon = \pm 1\%$. The following parameters are identified: $C_1, C_2, C_3, \gamma_1, \gamma_2$, the initial third backstress component $\chi_{3,0}$ and the yield stress σ_y. It is assumed the γ_3 component is linear ($\gamma_3 = 0$). Because the $\chi_{1,0}$ and $\chi_{2,0}$ parameters do not affect the stabilized behaviour, they do not calculated here. More information about the procedure is contained in [40]. The algorithm used in this paper is simplified as follows:

1) For each stabilized cycle used in the research, the plastic strain range $\Delta\varepsilon^p$, mean plastic strain $\varepsilon^{p,m}$, stress range of the stabilized cycle $\Delta\sigma$, mean stress of the stabilized cycle σ^m, the range of the stress for the stabilized cycle A and $\frac{d\sigma}{d\varepsilon^p}$ are determined at the extreme point using experimental data.
2) The c_3 and $\chi_{3,0}$ are calculated using Eq. 24 and 25.

$$C_3 = \frac{\sigma^{m,II} - \sigma^{m,I}}{\varepsilon_{II}^{p,m} - \varepsilon_I^{p,m}} \tag{24}$$

$$\chi_{3,0} = \frac{\varepsilon_{II}^{p,m}\sigma^{m,I} - \varepsilon_{I}^{p,m}\sigma^{m,II}}{\varepsilon_{II}^{p,m} - \varepsilon_{I}^{p,m}} \quad (25)$$

where: I and II means the first and the second hysteresis curve, $\chi_{3,0}$ is the initial value of the third backstress component.

3) The γ_1 trial values are assumed from the range of 100 to 2000.
4) The error function $\Psi(C_1, C_2, C_3, \gamma_1, \gamma_2, \chi_{3,0}, \sigma_y)$ which measures the fitting of a set of parameters, is computed.
5) For each trial value γ_1:
   - a_I, a_{II}, b_I and b_{II} values are computed using Eq. 26-29.

$$a_I = 1 - tanh\left(\frac{\gamma_1 \Delta\varepsilon_I^p}{2}\right) \quad (26)$$

$$a_{II} = 1 - tanh\left(\frac{\gamma_1 \Delta\varepsilon_{II}^p}{2}\right) \quad (27)$$

$$b_I = -C_3 + \left.\frac{d\sigma}{d\varepsilon^p}\right|_{\sigma=\sigma_{stab,I}^{max}} \quad (28)$$

$$b_{II} = -C_3 + \left.\frac{d\sigma}{d\varepsilon^p}\right|_{\sigma=\sigma_{stab,II}^{max}} \quad (29)$$

where: a_I, a_{II}, b_I and b_{II} are called dummy values for the determination of C_1 and C_2 parameters, $\sigma_{stab,I}^{max}$ and $\sigma_{stab,II}^{max}$ are maximum stress values read from a stabilized cycle for the first and the second hysteresis curves, respectively, $tanh$ is a hyperbolic tangent function.

   - The C_1 and C_2 values are computed with the use of Eq. 30-31.

$$C_1 = \frac{b_{II} - b_I}{a_{II} - a_I} \quad (30)$$

$$C_2 = \frac{a_{II}b_{II} - a_I b_I}{a_{II} - a_I} \quad (31)$$

   - The $\sigma_{y,I}$ and $\sigma_{y,II}$ value are calculated (Eq. 32-33).

$$\sigma_{y,I} = \frac{\Delta\sigma_I}{2} - \frac{C_1}{\gamma_1} tanh\left(\frac{\gamma_1 \Delta\varepsilon_I^p}{2}\right) - \frac{C_2 + C_3}{2}\Delta\varepsilon_I^p \quad (32)$$

$$\sigma_{y,II} = \frac{\Delta\sigma_{II}}{2} - \frac{C_1}{\gamma_1} tanh\left(\frac{\gamma_1 \Delta\varepsilon_{II}^p}{2}\right) - \frac{C_2 + C_3}{2}\Delta\varepsilon_{II}^p \quad (33)$$

   - The σ_y value is determined using Eq. 34.

$$\sigma_y = \frac{\sigma_{y,I} + \sigma_{y,II}}{2} \quad (34)$$

   - The error function Ψ is computed (Eq. 35).

$$\Psi(\gamma_1) = (1 - \alpha)\Sigma^2 + \alpha(\Lambda_I^2 + \Lambda_{II}^2) \quad (35)$$

where: α is a user parameter ($\alpha = 0.8$ here), Σ is the error function (Eq. 36), Λ_I and Λ_{II} is the error on the prediction of the hysteresis area of the first and the second cycles, respectively (Eq. 37-38).

$$\Sigma = \left|\frac{\sigma_{y,II} - \sigma_{y,I}}{\sigma_y}\right| \quad (36)$$

$$\Lambda_I = \frac{2\sigma_y \Delta\varepsilon_I^p + 2\left(\frac{C_1}{\gamma_1}\Delta\varepsilon^p - 2\frac{C_1}{\gamma_1^2} tanh\left(\frac{\gamma_1 \Delta\varepsilon^p}{2}\right)\right)}{A_I} - 1 \quad (37)$$

$$\Lambda_{II} = \frac{2\sigma_y \Delta\varepsilon_{II}^p + 2\left(\frac{C_1}{\gamma_1}\Delta\varepsilon^p - 2\frac{C_1}{\gamma_1^2} tanh\left(\frac{\gamma_1 \Delta\varepsilon^p}{2}\right)\right)}{A_{II}} - 1 \quad (38)$$

where: A_I and A_{II} are areas of the hysteresis loop of I and II stabilized cycles (Eq. 39).

$$A_I = A_{II} = 2\sigma_y \Delta\varepsilon^p + 2\left(\frac{C_1}{\gamma_1}\Delta\varepsilon^p - 2\frac{C_1}{\gamma_1^2} tanh\left(\frac{\gamma_1 \Delta\varepsilon^p}{2}\right)\right) = \oint \sigma d\varepsilon^p \quad (39)$$

6) The γ_1 parameter is selected for which the error function Ψ is the minimum and the other parameters are updated.
7) The γ_2 is assumed to be in the range of 1÷2000 to metal alloys in line with the procedure proposed by Santus et al. [40].
8) The Q and b isotropic hardening parameters are determined using Eq. 40-42.

$$Q = \sigma_y - \sigma_{y,0} \quad (40)$$

$$\sigma_{y,0} - \sigma_y = -Qexp(-bp) \quad (41)$$

$$p = \int |d\varepsilon^p| \quad (42)$$

Using the steps presented above, the algorithm is also written in a commercial program and then used.

Experimental research

The symmetrical total strain-control cyclic tension-compression tests with different $\Delta\varepsilon$ strain range were carried out in order to determine the hardening parameters for CIKH model. The research was carried out on a hydraulic universal testing machine (Z100 ZWICK ROELL, Germany) at ambient temperature (Fig. 4). The cyclic tension-compression tests were carried out for a construction steel S235JR which is commonly used in a construction sector. The chemical composition of steel applied is contained in Table 1. The selected mechanical properties, e.g. the Young modulus and the initial yield stress were determined using the first half-loaded part of the hysteresis loop.

During the experiment, the symmetrical deformation $\varepsilon = \pm 1\%$ and $\varepsilon = \pm 1.5\%$, as well as,

a)

b)

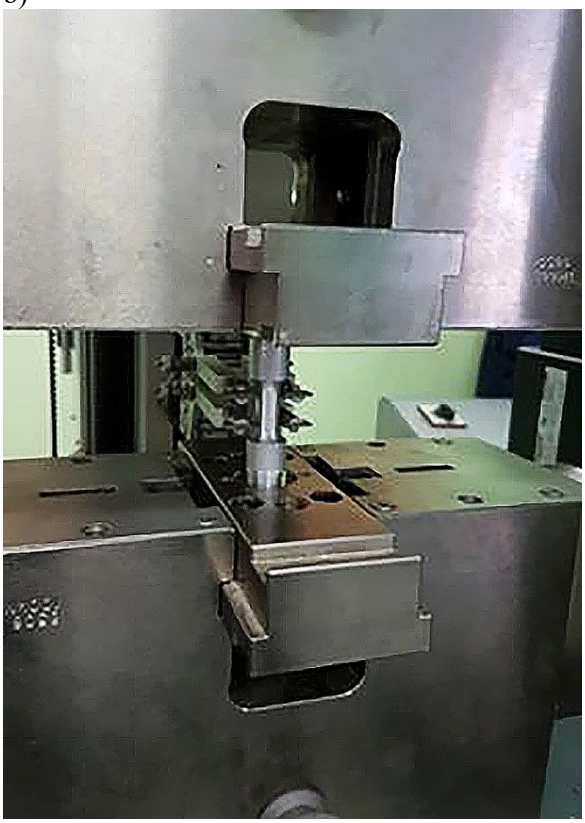

Figure 4. The universal testing machine used in the research (a) and the sample during the test (b)

Table 1. Chemical composition of S235JR steel used in the research

Compound	C	Mn	P	S	Cu	N
Percentage [%]	0.17	1.40	0.035	0.035	0.55	0.012

non-symmetrical deformation $\varepsilon = -0.5 \div 1\%$ of the 15 mm measuring base is used. The hourglass samples were prepared from 12 mm diameter rolled bars (Fig. 5). The elongation of the specimen was measured during the cyclic loading tests using the extensometer (ZWICK ROELL, Germany). The obtained force-elongation curve is transferred then into stress-strain one.

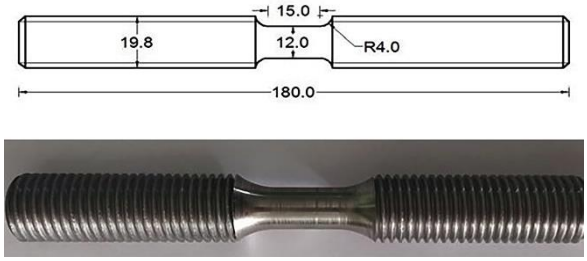

Figure 5. The sample used in the cyclic loading test

RESULTS AND DISCUSSION

Identification of hardening parameters

Firstly, some mechanical properties – the initial yield stress (σ_{y0}) and the Young modulus (E), necessary for the identification procedure, are determined. These values are read from the half loaded part of the first hysteresis loop (Fig. 6). The following mechanical parameters are read: the initial yield stress σ_{y0} = 235 MPa and Young modulus E = 193 GPa.

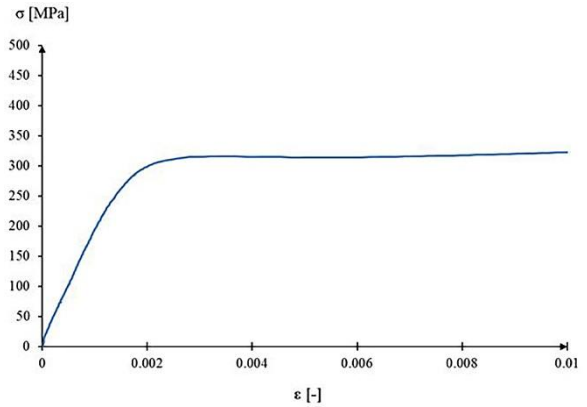

Figure 6. The half loaded part of the first hysteresis loop ($\varepsilon = \pm 1\%$)

The strain-controlled cyclic loading tests were carried out until the stabilization of the curve was achieved. Therefore, the sample was subjected to 6 load cycles. It was noted that the material indicates both isotropic and kinematic hardening associated with the increase and the translation of a yield surface, respectively.

The experimental stress-strain curves obtained for S235JR construction steel during the cyclic tension-compression tests under strain-control conditions for different strains tested is shown in Figure 7. The hysteresis curve for $\varepsilon = \pm 1\%$ is used further in order to determine the hardening parameters and then, the parameters were applied in order to model curves for other strains. The last stabilized cycle selected from the hysteresis curve which is used for the parameter identification is presented in Figure 8.

The procedures for the determination of both isotropic and kinematic hardening parameters is carried out according to the previous section of the paper. Firstly, the method based on the last stabilized cycle of the hysteresis curve is tested. The CIKH hardening parameters obtained are contained in Table 2. Three non-linear kinematic components are selected here. In order to check

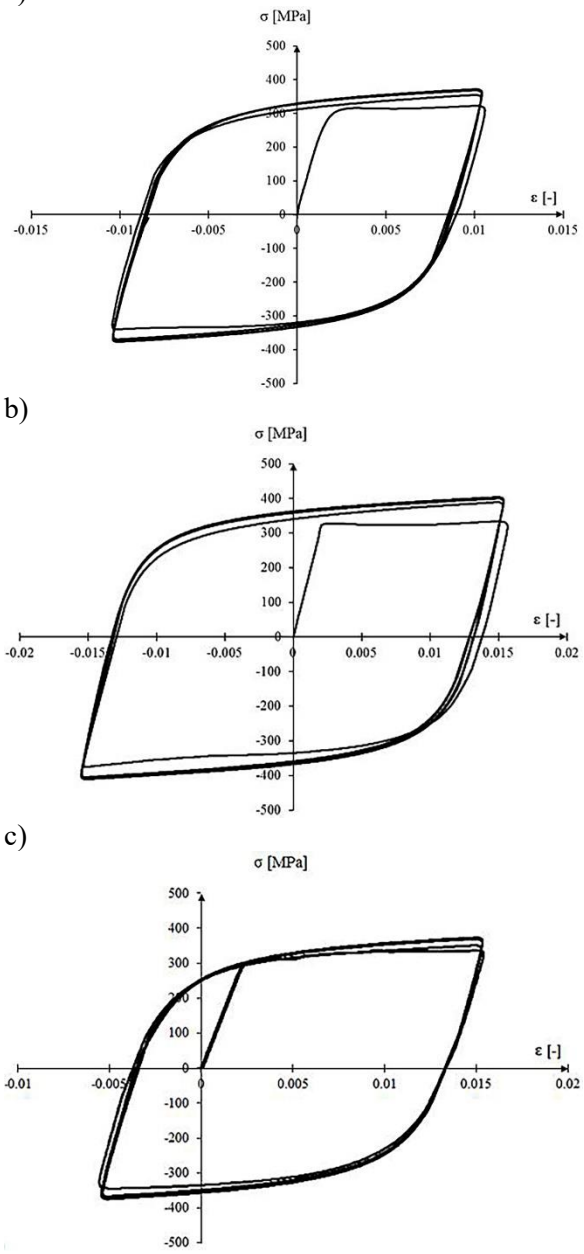

Figure 7. The stress-strain curves showing hysteresis loops obtained in strain-controlled cyclic loading tests for $\varepsilon = \pm 1\%$ (a), $\varepsilon = \pm 1.5\%$ (b) and for non-symmetrical test ($\varepsilon = -0.5 \div 1\%$) (c)

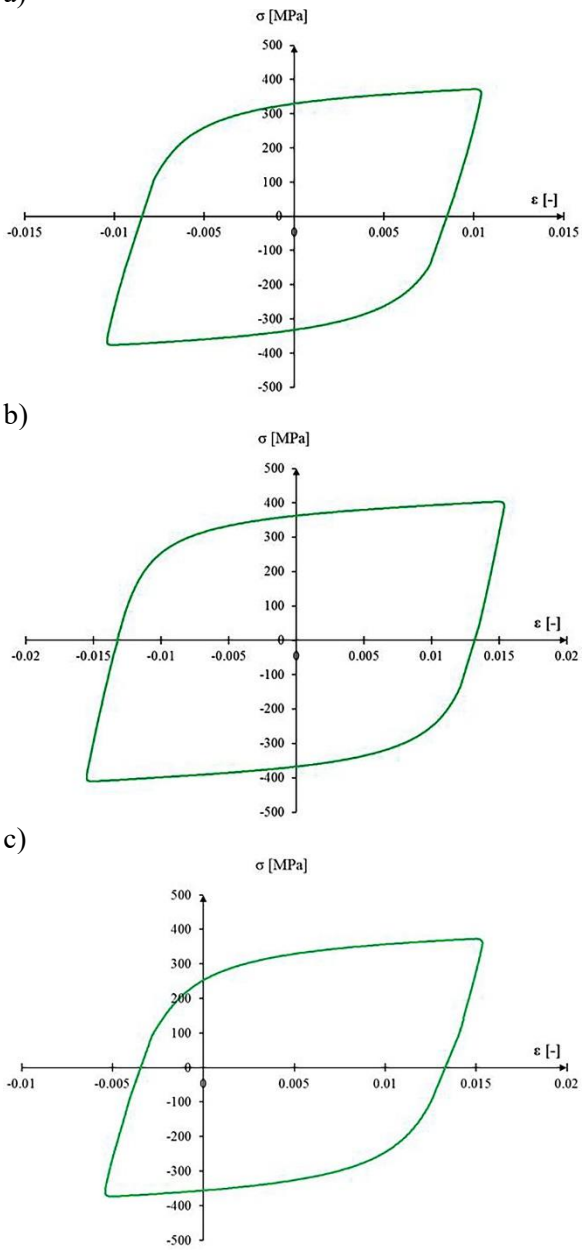

Figure 8. The last stabilized cycle for the strain-controlled cyclic loading test; $\varepsilon = \pm 1\%$ (a), $\varepsilon = \pm 1.5\%$ (b) and for non-symmetrical test ($\varepsilon = -0.5 \div 1\%$) (c)

Table 2. Hardening parameters of the CIKH model using the last stabilized cycle procedure

Hardening parameter	Isotropic hardening		Kinematic hardening					
	Q [MPa]	b [-]	C_1 [MPa]	γ_1 [-]	C_2 [MPa]	γ_2 [-]	C_3 [MPa]	γ_3 [-]
Value	132.0	3.0	2021.0	279.0	4157.0	87.7	4191.0	11.4

effects of the procedure applied, the numerically-generated stress-strain curve on the basis of the determined hardening parameters, is compared to the experimental data (Fig. 9). The good convergence between both curves is noted at this stage without any optimization procedure. It is quite evident that the last regions of the curve are modeled the best which is associated with the identification procedure applied. In the stabilized cycle method, the hardening parameters are selected using only the last stabilized cycle. The inaccurate is observed in corners of the hysteresis curve.

a)

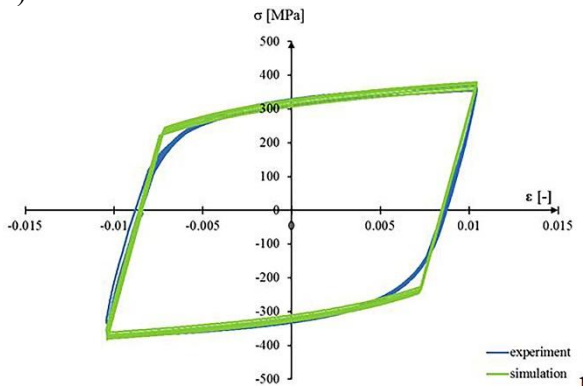

b)

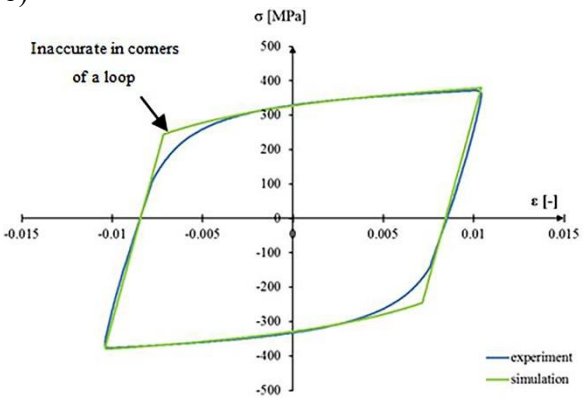

Figure 9. The comparison of experimental and numerical curves for the last stabilized cycle procedure (a) and the fitting to the last stabilized cycle (b)

The hardening parameters determined for $\varepsilon = \pm 1\%$ were then applied in the simulation of hysteresis curves for other tested strains (symmetrical $\varepsilon = \pm 1.5\%$ and non-symmetrical $\varepsilon = -0.5 \div 1\%$) in order to check if hardening parameters determined in $\Delta\varepsilon = \pm 1\%$ provide a reasonable approximation for another cases. The results obtained are shown in Figure 10 and Figure 11. The confirmation of good agreement between numerically-generated and experimental curves for all cases indicates the possibility of the reduction of the number of the experimental research which is important from the economic point of view.

a)

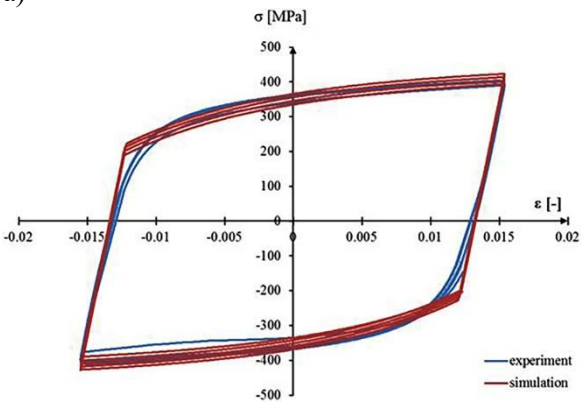

b)

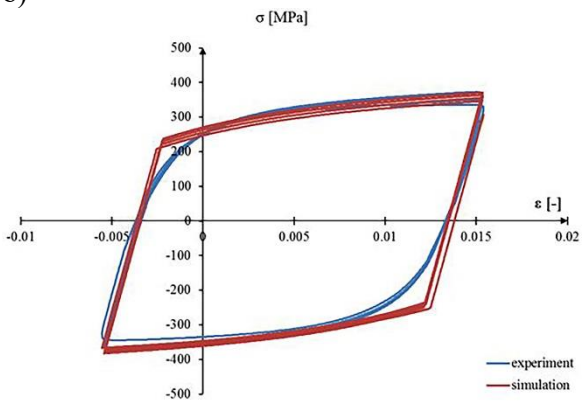

Figure 10. The comparison of experimental and numerical curves for the last stabilized cycle procedure for $\varepsilon = \pm 1.5\%$ (a) and for $\varepsilon = -0.5 \div 1\%$ (b)

After that, the procedure proposed by Santus et al. [40] was tested in this paper. The method was applied for the hysteresis curve obtained for $\varepsilon = \pm 1\%$. The hardening parameters used in this algorithm is contained in Table 3. The Figure 12 shows the similarities and differences between experimental and numerical hysteresis loops. It is shown that the better results are obtained using the last stabilized method. Especially, the differences between two tested procedures are visible

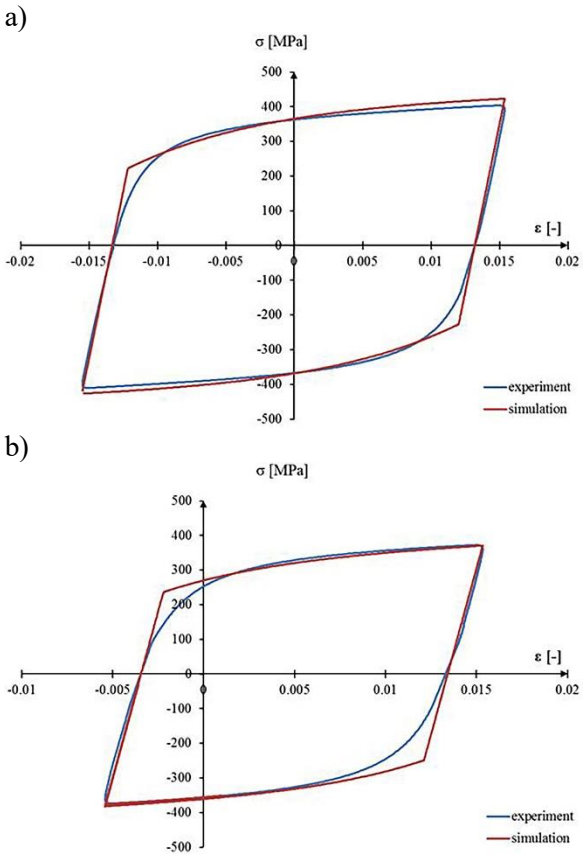

Figure 11. The comparison of experimental and numerical curves for the last stabilized cycle procedure for $\varepsilon = \pm 1.5\%$ (a) and for $\varepsilon = -0.5 \div 1\%$ (b) (the last stabilized cycle only)

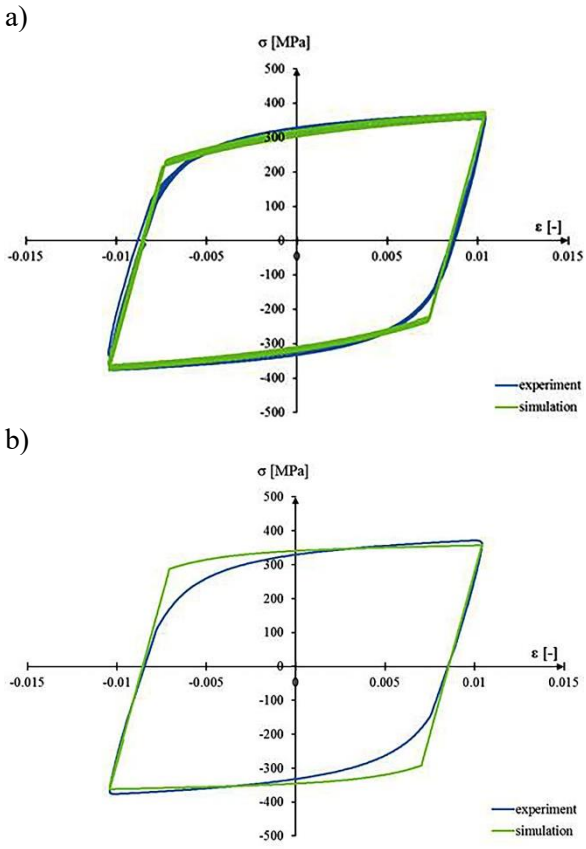

Figure 12. The comparison between experimental and numerically-generated curves for the procedure proposed by Santus et al. [40] for $\varepsilon = \pm 1\%$ (a) and the fitting to the last stabilized cycle (b)

for stabilized cycles. The parameters for the first tested procedure are then used in the optimization procedure.

Using the authorial algorithm based on the last stabilized cycle method, the additional information about the change of total backstress, as well as, the isotropic hardening in time is obtained (Fig. 13). The non-linear isotropic and kinematic hardening, as well as the saturation of the isotropic one, is noted.

Optimization procedure

In order to improve the agreement between experimental and numerically-generated hysteresis curves, the optimization procedure is applied in this research. Recently, different optimization methods has been tested [53-56]. The optimization technique using the least-square approach is proposed here. The procedure was written in a commercial program and tested previously by authors [20]. Due to its effectiveness of the improvement of the convergence between numerical and experimental data, the method is also applied in this paper. The idea of the least-square optimization method is the minimizing the error of estimation between experimental and numerical data. The technique is described in more detail in [57-59]. The error $\|Z\|$ is computed as follows (Eq. 43):

$$\|Z\| = \sqrt{\int_0^{\varepsilon_{max}} (\sigma_{exp} - \sigma_{num})^2 d\varepsilon} \qquad (43)$$

where: ε_{max} is the experimentally obtained maximum value of the strain, σ_{exp} – stress registered

Table 3. Hardening parameters of the CIKH model for S235JR steel using the procedure proposed by Santus et al. [40]

Hardening parameter	Isotropic hardening		Kinematic hardening					
	Q [MPa]	b [-]	C_1 [MPa]	γ_1 [-]	C_2 [MPa]	γ_2 [-]	C_3 [MPa]	γ_3 [-]
Value	132.0	3.0	2189	300.0	4500.3	100.0	4150.0	0.0

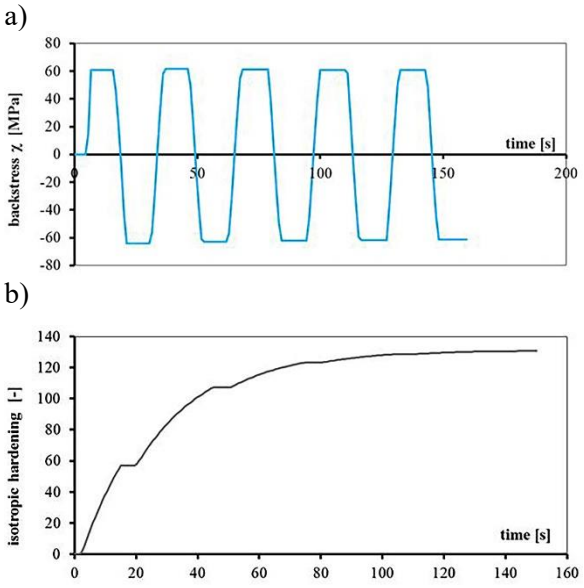

Figure 13. The change of backstresses (a) and isotropic hardening (b)

during the experiment, σ_{num} – stress obtained in numerical calculations. The σ_{num} value is estimated using the hardening parameters.

In such authorial algorithm, the hardening parameters initially determined are randomly scattered up to 10% and for each set of them, the σ_{num} and the $\|Z\|$ are calculated. The hardening parameters determined using the least-square method for which the error is the smallest, are contained in Table 4. The exemplary results for hysteresis curve for $\varepsilon = \pm 1\%$ is shown in Figure 14. The slightly improvement between such numerically-generated and experimental curves is observed what shows that the initial selection of hardening parameters was done correctly. The error norm decreases form $\|Z\|$= 33 MPa to $\|Z\|$= 10 MPa. However, the improvement of the fitting in corners of hysteresis loops is not noted.

The application of a fuzzy logic approach

As mentioned before, the selection of CIKH model hardening parameters is often subjected to some errors associated both with the experiment prediction, as well as, the identification procedure. In order to improve the convergence between experiment and numerical results, different

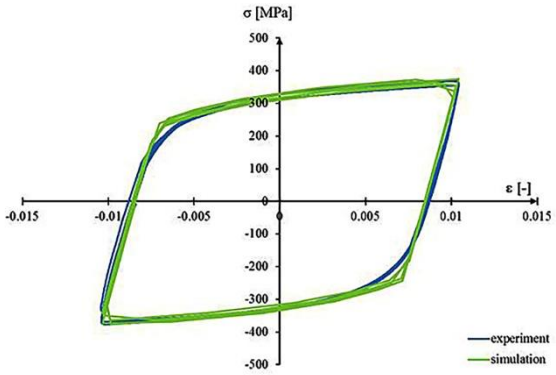

Figure 14. The comparison of experimental and numerical curves after the use of the least-square method

optimization techniques are tested. However, as it proved in authors previous paper, the similar error can be obtained for many different sets of parameters. Additionally, the some uncertainty of experimental data and the material model applied should be included.

In order to determine the most reliable solution without many experiments, the method based on the fuzzy logic is applied by authors. The fuzzy logic is, as a genetic algorithm, a soft-computing method which assumes some uncertainty of input and output data, as well as, the uncertainty of a mapping model. More details about fuzzy logic is contained in [60-63].

The authorial procedure based on fuzzy set theory was written and tested previously by the authors [20, 21]. Due to its effectiveness for the determination of the most reliable values of hardening parameters, it is also contained here. The fuzzy input variables were initially determined hardening parameters and the fuzzy output one was the $\|Z\|$ error. The set of constitutive equations of CIKH model is used as a mapping model. The procedure for the identification of hardening parameters on the basis of the fuzzy logic is summarized in line with the following steps:

1) The parameters related to isotropic and kinematic hardening, which are fuzzy input variables, are fuzzified and membership functions are constructed for them. Different shapes of membership functions were tested but the results for triangular membership functions are presented here.

Table 4. Hardening parameters of the CIKH model for S235JR steel after the use of the least-square method

Hardening parameter	Isotropic hardening		Kinematic hardening						‖Z‖ [MPa]
	Q [MPa]	b [-]	C_1 [MPa]	γ_1 [-]	C_2 [MPa]	γ_2 [-]	C_3 [MPa]	γ_3 [-]	
Value	124.3	2.7	1994.7	210.6	3632.9	83.3	3244.2	6.6	10

2) The membership functions obtained are divided into several number of α-levels for the α-level method applied here.
3) The boundary C_i, γ_i, b and Q values are selected for a certain α-level of all membership functions.
4) Minimum and maximum values of $\|Z\|$ error are computed for all input parameters using Eq. 44. These values determine shapes of the output membership functions.

$$\begin{cases} \|Z\| = f(Q, b, C_i, \gamma_i) \Rightarrow \min(Q, b, C_i, \gamma_i) \in X_{\alpha k} \\ \|Z\| = f(Q, b, C_i, \gamma_i) \Rightarrow \max(Q, b, C_i, \gamma_i) \in X_{\alpha k} \end{cases} \quad (44)$$

where: requirements $(Q, b, C_i, \gamma_i) \in X_{\alpha k}$ describes constraints for the optimization method.

5) The discrete Z_0 value is calculated in the defuzzification step using the mass center (Eq. 45), the centroid (Eq. 46) and the level rank (Eq. 47) methods in order to check the influence of the defuzzification method on final results. Such obtained Z_0 value is the most reliable solution.

$$Z_0 = \frac{\int Z \cdot \mu(Z) dZ}{\int \mu(Z) dZ} \quad (45)$$

$$Z_0 = \int_Z Z \cdot \mu(Z) dZ \cdot \left[\int_Z \mu(Z) dZ \right]^{-1} \quad (46)$$

$$Z_0 = \frac{1}{r} \cdot \sum_{k=1}^{r} \frac{Z_{\alpha_{k_l}} + Z_{\alpha_{k_r}}}{2} \quad (47)$$

where: r is a number of α-levels assumed, $Z_{\alpha_{k_l}}$ and $Z_{\alpha_{k_r}}$ are boundaries of α-levels considered.

6) The most reliable solution is a set of hardening parameters with the minimal error Z_0.

The hardening parameters obtained using the fuzzy logic algorithm are listed in Table 5. For such parameters obtained, the numerical hysteresis stress-strain curve is generated which is then compared with the experimental one. The exemplary results for hysteresis curve for $\varepsilon = \pm 1\%$ is shown in Figure 15. Due to the fact that similar hardening parameters are obtained and the hysteresis curves are very similar (differences are not visible), the results for the mass center method are only shown. A good agreement between the curves is noted. Although, the fuzzy logic procedure does not improve the fitting of experimental and numerical hysteresis loops significantly, the algorithm includes the impact of the constitutive equations of theory of plasticity on the results. In comparison, it is not contained in a pure statistical approach.

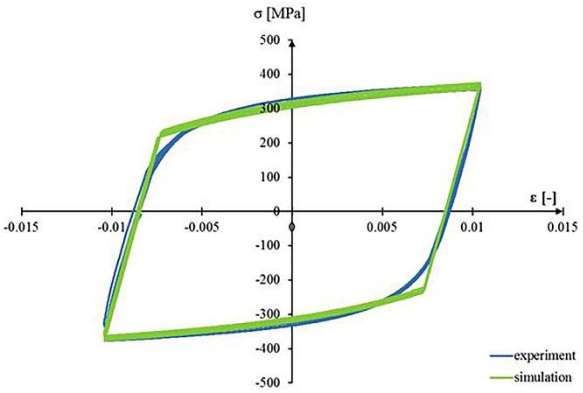

Figure 15. The comparison between experimental and numerical curves after the use of the fuzzy set theory algorithm (the mass center deffuzification method)

CONCLUSIONS

The modelling of the material behaviour under loading requires the right selection of the material model, as well as, the right identification of hardening parameters. However, for models with a several parameters, e.g. the Chaboche-Lemaitre combined isotropic-kinematic hardening model with some backstresses, the identification of the hardening parameters is a complex and time-consuming process. The procedure of the selection the isotropic and kinematic hardening parameters for the Chaboche-Lemaitre combined isotropic-kinematic

Table 5. Hardening parameters for S235JR steel after the use of a fuzzy logic algorithm and different deffuzification methods

Hardening parameter	Isotropic hardening		Kinematic hardening						‖Z‖ [MPa]
	Q [MPa]	b [-]	C_1 [MPa]	γ_1 [-]	C_2 [MPa]	γ_2 [-]	C_3 [MPa]	γ_3 [-]	
The mass center method									
Value	125.3	2.9	2005.7	200.6	3442.5	80.2	3124.5	6.7	8.7
The centroid method									
Value	121.7	2.6	1924.5	191.5	3329.5	79.5	2998.1	5.9	9.1
The level rank method									
Value	126.0	3.0	2134.6	210.5	3423.6	89.3	3055.5	6.2	9.0

hardening model (CIKH) based on the experimental data obtained in a strain-controlled cyclic loading test for S235JR construction steel is applied in this paper. This material was analyzed here due to the fact that it is subject to cyclic loading during its application in a construction sector.

The selection of hardening parameters is done using the last stabilized cycle of a hysteresis curve obtained in a cyclic loading test. The good convergence between experimental data and numerical calculations is obtained. For the improvement of the convergence between experiment and numerical calculations, the least-square optimization procedure was tested. For the selection of the most reliable solution, an authorial procedure written on the basis of the fuzzy logic was also applied. Based on the results obtained in this paper, the main conclusions are as follows:

1. The identification procedure for the CIKH model gives a set of isotropic and kinematic parameters with a good agreement with the experimental data. However, slightly better fitting between experimental and numerical data is achieved for the last stabilized cycle procedure.
2. The hardening parameters determined under the symmetrical stain-controlled cyclic loading test for =1% can be applied for modelling of hysteresis curves for other strains with good results. Therefore, the number of experimental research can be reduced to the minimum.
3. The optimization algorithm can improve the convergence between the experiment and numerical simulations by minimizing the error norm.
4. The advantage of the authorial algorithm is the possibility to achieve additional information about the hardening, e.g. the change of the backstress in time.
5. The selection of hardening parameters is subject to some error associated with both experiment and the identification procedure. In order to include some uncertainty of input data and model applied, as well as including the mapping model, the authorial algorithm based on the fuzzy logic is tested.
6. The results obtained using the fuzzy logic procedure are similar to the results of pure statistics. However, the approach based on the fuzzy theory does not require a lot of experimental data. It is the additional advantage of the method proposed.
7. The correct determination of hardening parameters is essential for modelling phenomena occurring in the material during different processes, including metal forming processes.

In further research, the application of other soft-computing method, e.g. genetic algorithm will be tested in order to select the right values of hardening parameters. The other models will be also tested in modelling of the cyclic stress-strain hysteresis curves, e.g. Ohno-Wang model or modified Chaboche ones.

Acknowledgement

The research leading to these results has received funding from the commissioned task entitled "VIA CARPATIA Universities of Technology Network named after the President of the Republic of Poland Lech Kaczyński" contract no. MEiN/2022/DPI/2578 action entitled "In the neighborhood – inter-university research internships and study visits".

REFERENCES

1. Rippan R., Hohenwarter A. Fatigue crack closure: a review of the physical phenomena. Fatigue & Fracture of Engineering Materials & Structures 2017; 40(4): 471-495.
2. Resapu R.R., Perumahanthi L.R. Numerical study of bilinear isotropic & kinematic elastic-plastic response under cyclic loading. Materials Today: Proceedings 2021; 39(4): 1647-1654.
3. Hashemi E., Farshi B. Cyclic Loading of Beams Based on Kinematic Hardening Models: A Finite Element Approach. International Journal of Modeling and Optimization 2011; 1(3): 210-215.
4. Mahbadi H., Eslami M.R. Cyclic loading of beams based on Prager and Frederick-Armstrong kinematic hardening models. International Journal of Mechanical Sciences 2002; 44(5): 859-879.
5. Shojaei A.K., Eslami M.R., Mahbadi H. Cyclic loading of beams based on the Chaboche model. International Journal of Mechanical Sciences 2010; 6(3): 217-228.
6. Xing R., Yu D., Shi S., Chen X. Cyclic deformation of 316L stainless steel and constitutive modeling under non-proportional variable loading path. International Journal of Plasticity 2019; 120: 127-146.
7. Bai J., Jin K., Kou Y. Loading history effect on ratcheting behaviour: Modelling and simulation. International Journal of Mechanical Sciences 2023; 252: 108379.
8. Kobelev V. Some basic solutions for nonlinear creep. International Journal of Solids and Structures 2014; 51(19-20): 3372-3381.
9. Suchocki C., Kowalewski Z. A new method for identification of cyclic plasticity model parameters. Archives of Civil and Mechanical Engineering 2022; 22: 69.

10. Wójcik M., Skrzat A. Coupled Thermomechanical Eulerian-Lagrangian Analysis of the KOBO Extrusion Process. Archives of Metallurgy and Materials 2022; 67(3): 1185-1193.
11. Wójcik M., Skrzat A. The Coupled Eulerian-Lagrangian Analysis of the KOBO Extrusion Process. Advances in Science and Technology Research Journal 2021; 15(1): 197-208.
12. Mahmoudi A.H., Badnava H., Pezeshki-Najafabadi S.M. An application of Chaboche model to predict uniaxial and multiaxial ratcheting. Procedia Engineering 2011; 10: 924-1929.
13. Xu X., Wang Z., Zhang X., Gao G., Wang P., Kan Q. Strain amplitude-dependent cyclic softening behaviour of carbide-free bainitic rail steel: Experiments and modeling. International Journal of Fatigue 2022; 161: 106922.
14. Zobec P., Klemenc J. Application of a nonlinear kinematic-isotropic material model for the prediction of residual stress relaxation under a cyclic load. International Journal of Fatigue 2021; 150: 106290.
15. Wagoner R.H., Lim H., Lee M.-G. Advanced Issues in springback. International Journal of Plasticity 2013; 45: 3-20.
16. Xue L., Shang D.G., Li D.-H., Xia Y. Unified Elastic-Plastic Analytical Method for Estimating Notch Local Strains in Real Time under Multiaxial Irregular Loading. Journal of Materials Engineering and Performance 2021; 30: 9302-9314.
17. Zhu Y., Kang G., Kan Q., Bruhns O., Liu Y. Thermomechanically coupled cyclic elasto-viscoplastic constitutive model of metals: Theory and application. International Journal of Plasticity 2016; 76: 111-152.
18. Liu S., Liang G., Yang Y. A strategy to fast determine Chaboche elasto-plastic model parameters by considering ratcheting. International Journal of Pressure Vessels and Piping 2019; 172, 251-260.
19. Hai L.-T., Li G.-Q., Wang Y.-B., Wang Y.-Z. A fast calibration approach of modified Chaboche hardening rule for low yield point steel, mild steel and high strength steels. Journal of Building Engineering 2021; 38: 102168.
20. Wójcik M., Skrzat A. Identification of Chaboche-Lemaitre combined isotropic-kinematic hardening model parameters assisted by the fuzzy logic analysis. Acta Mechanica 2021; 232: 685-708.
21. Wójcik M., Skrzat A. Fuzzy logic enhancement of material hardening parameters obtained from tension-compression test. Continuum Mechanics and Thermodynamics 2020; 32: 959-969.
22. Lee C.-H., Do V.N.V., Chang K.-H. Analysis of uniaxial ratcheting behavior and cyclic mean stress relaxation of a duplex stainless steel. International Journal of Plasticity 2014; 62: 17-33.
23. Agius D., Kajtaz M., Kourousis K.I., Wallbrink C., Wang C.H., Hu W., Silva J. Sensitivity and optimization of the Chaboche plasticity model parameters is strain-life fatigue predictions. Materials & Design 2017; 118: 107-121.
24. Ding J., Kang G., Kan Q., Liu Y. Constitutive model for uniaxial time-dependent ratcheting of 6061-T6 aluminum alloy. Computational Materials Science 2012; 57: 67-72.
25. Hamidinejad S.M., Varvani-Farahani A. Ratcheting assessment of steel samples under various non-proportional loading paths by means of kinematic hardeningnrules. Materials & Design 2015; 815, 367-376.
26. Moslemi N., Zardian M.G., Ayob A., Redzuan N., Rhee S. Evaluation of Sensitivity and Calibration of the Chaboche Kinematic Hardening Model Parameters for Numerical Ratcheting Simulation. Applied Science 2019; 9(12): 2578.
27. Cao W., Yang J., Zhang H. Unified constitutive modeling of Haynes 230 including cyclic hardening/softening and dynamic strain aging under isothermal low-cycle fatigue and fatigue-creep loads. International Journal of Plasticity 2021; 138: 102922.
28. Burgold A., Droste M., Seupel A., Budnitzki M., Biermann H., Kuna M. Modeling of the cyclic deformation behaviour of austenitic TRIP-steels. International Journal of Plasticity 2020; 133: 102792.
29. Egner W., Sulich P., Mroziński S., Egner H. Modelling thermo-mechanical cyclic behavior of P91 steel. International Journal of Plasticity 2020; 135: 102820.
30. Okorokov V., Gorash Y., Mackenzie D., van Rijswick R. New formulation of nonlinear kinematic hardening model, Part II: Cyclic hardening/softening and ratcheting. International Journal of Plasticity 2019; 122: 244-267.
31. Hwang J.-H., Kim H.-T., Kim Y.-J., Nam H.-S., Kim J.-W. Crack tip field at crack initiation and growth under monotonic and large amplitudę cycle loading: Experimental and FE analyses. International Loading of fatigue 2020; 141: 105889.
32. Song Z., Komvopoulos K. An elastic-plastic analysis of spherical indentation: Constitutive equations for single-indentation unloading and development of plasticity due to repeated indentation. Mechanics of Materials 2014; 76: 93-101.
33. Lam Wing Cheong M.F., Rouse J.P., Hyde C.J., Kennedy A.R. The Prediction of isothermal cyclic plasictity in 7175-T7351 aluminium alloy with particular emphasis on thermal ageing effects. International Journal of Fatigue 2018; 114: 92-108.
34. Esmaeili A., Walia M.S., Handa K., Ikeuchi K., Ekh M., Vernersson T., Ahlström J. A methodology to predict thermomechanical cracking of railway wheel treads: From experiments to numerical predictions. International Journal of Fatigue 2017; 105: 71-85.
35. Abueidda D.W., Koric S., Sobh N.A., Sehitoglu H. Deep learning for plasticity and thermos-viscoplasticity. International Journal of Plasticity 2021; 136: 02852.

36. Nath A., Ray K.K. Barai S.V. Evaluation of ratcheting behaviour in cyclically stable steels through use of a combined kinematic-isotropic hardening rule and a genetic algorithm optimization technique. International Journal of Mechanical Sciences 2019; 152: 138-150.
37. Nath A., Barai S.V., Ray K.K. Studies on the experimental and simulated cyclic-plastic response of structural mild steels. Journal of Constructional Steel Research 2021; 182: 106652.
38. Badnava H., Pezeshki S.M., Nejad K.F., Farhoudi H.R. Determination of combined hardening material parameters under strain controlled cyclic loading by using the genetic algorithm method. Journal of Mechanical Science and Technology 2012; 26: 3067-3072.
39. Skrzat A., Wójcik M. An identification of the material hardening parameters for cyclic loading – experimental and numerical studies. Archives of Metallurgy and Materials 2020; 65(2): 779-786.
40. Santus C. Grossi T., Romanelli L., Pedranz M., Benedetti M. A computationally fast and accurate procedure for the identification of the Chaboche isotropic-kinematic hardening model parameters based on strain-controlled cycles and asymptotic ratcheting rate. International Journal of Plasticity 2023;160: 103503.
41. Chaboche J.L. Time-independent constitutive theories for cyclic plasticity. International Journal of Plasticity 1986; 2(2): 149-188.
42. Mahmoudi A.H., Pezeshki-Najafabadi S.M., Badnava H. Parameter determination of Chaboche kinematic hardening model using a multi objective Genetic Algorithm. Computational Materials Science 2011; 50(3):1114-1122,
43. Srnec Novak J., De Bona F., Benasciutti D. Benchmarks for accelerated cyclic plasticity models with finite elements. Metals 2020; 10(6): 781.
44. Borges M.F., Antunes F.V., Prates P.A., Branco R.A Numerical study of the effect of isotropic hardening parameters on mode I fatigue crack growth. Metals 2020; 10(2): 177.
45. Szala M., Winiarski G., Bulzak T., Wójcik Ł. Microstructure and hardness of cold forged 42CrMo4 steel hollow component with the outer flange. Advances in Science and Technology Research Journal 2022; 16(4): 201-210.
46. Chaboche, J.L. Modeling of ratcheting: evolution of various approaches. European Journal of Mechanics A/Solids 1994; 13: 501-518.
47. Chaboche J.L. A review of some plasticity and viscoplasticity constitutive theories. International Journal of Plasticity 2008; 24:1642–1693.
48. Bari S., Hassan T. An advancement in cyclic plasticity modeling for multiaxial ratcheting simulation. International Journal of Plasticity 2008; 18(7): 873-894.
49. Rezaiee-Pajand M., Sinaie S. the number of back-stresses above 3 is not necessary and the application of their higher number does not improve the convergence between experimental and numerical data. International Journal of Solids and Structures 2009; 46(16): 3009-3017.
50. Welling C.A., Marek R., Feigenbaum H.P., Dafalias Y.F., Plesek J., Hruby Z., Parma S. Numerical convergence in simulations of multiaxial ratcheting with directional distortional hardening, International Journal of Solids and Structures 2017; 126-127: 105-121.
51. Dvoršek N., Stopeinig I., Klančnik S. Optimization of Chaboche Material Parameters with a Genetic Algorithm. Materials 2023;16(5): 1821.
52. Gomes V.M.G., Eck S., De Jesus A.M.P. Cyclic hardening and fatigue damage features of 51CrV4 steel for the crossing nose design. Applied Sciences 2023; 13: 8308.
53. Chaparro B.M., Thuillier S., Menezes L.F., Manach P.Y., Fernandes J.V. Material parameters identification: Gradient-based, genetic and hybrid optimization algorithms. Computational Materials Science 2008; 44(2): 339–346.
54. Sinaie S., Heidarpour A., Zhao X.L. A multi-objective optimization approach to the parameter determination of constitutive plasticity models for the simulation of multi-phase load histories. Computers & Structures 2014; 138: 112–132.
55. Petry A., Gallo P., Remes H., Niemelä A. Optimizing the Voce–Chaboche model parameters for fatigue life estimation of welded joints in high-strength marine structures. Journal of Marine Science and Engineering 2022; 10(6): 818.
56. Liu S., Guozhu L. Optimization of Chaboche kinematic hardening parameters by using an algebraic method based on integral equations. Journal of Mechanics of Materials and Structures 2017; 12(4): 439-455.
57. Tsai, K., Chiu, C.: Computer-aided photoelastic analysis of orthogonal 3D textile composites: Part 2. Combining least squares and finite-element methods for stress analysis. Experimental Mechanics 1998; 38: 8-12.
58. Overall J.E., Spiegel, D.K. Concerning least squares analysis of experimental data. Psychological Bulletin 1969; 72(5): 311-322.
59. Usami M., Oya T. Estimation of work-hardening curve for large strain using friction- free compression test. Proceedia Engineering 2014; 81: 371-376.
60. Koutsianitis P., Tairidis G.K., Drosopoulos G.A., Foutsitzi G.A., Stavroulakis G.E. Effectiveness of optimized fuzzy controllers on partially delaminated piezocomposites. Acta Mechanica 2017; 228: 1373-1392.
61. Brooks L. Fuzzy Logic: Theory and Applications. Larsen and Keller Education, 2017.
62. Shahbazova S.N., Sugeno M., Kacprzyk J. Recent developments in fuzzy logic and fuzzy sets. Springer, 2020.
63. Möller, B., Beer, M. Fuzzy Randomness. Uncertainty in civil engineering and computational mechanics. Springer, 2004.